JOURNAL OF Materials CHEMISTRY

Structural and computational studies of Bi_2WO_6 based oxygen ion conductors

M. Saiful Islam,[a] Sylvie Lazure,[b] Rose-Noëlle Vannier,[b] Guy Nowogrocki[b] and Gaëtan Mairesse*[b]

[a]*Department of Chemistry, University of Surrey, Guildford, UK GU2 5XH*
[b]*Laboratoire de Cristallochimie et Physicochimie du Solide, ENSCL-USTLille, URA 452, B.P. 108, 59652 Villeneuve d'Ascq Cedex, France*

A combination of neutron powder diffraction and computer simulation techniques was performed on undoped and doped Bi_2WO_6 Aurivillius type compounds to clarify some of the factors controlling oxygen transport in these materials. Oxygen vacancies in doped compounds are randomly distributed within the perovskite-like slab. The most favourable dopants are predicted to be Nb^V and Ta^V on W^{VI} and La^{III} on Bi^{III} in accordance with the experimental results. The calculated migration energy of 0.63 eV is in agreement with the values deduced from impedance spectroscopy data for Ta and Nb doped Bi_2WO_6 at $T > 550\,^{\circ}C$. At lower temperatures, pair clusters are predicted to form with a 0.25 eV mean binding energy, leading to a 0.88 eV activation energy for oxygen vacancy migration, in good correlation with experimental values. Finally, consideration of possible oxygen ion migration pathways in the structure showed that energy barriers to migration are lowest between adjacent apical and equatorial sites of WO_6 oxygen octahedra.

The oxides of the Aurivillius family, of general formula $(Bi_2O_2)(A_{m-1}B_mO_{3m+1})$ were originally of interest for their ferroelectric properties but have recently been explored in the field of oxide ion conductivity and constitute now an important new class of oxide anion conductors.[1] The Aurivillius phases consist of an intergrowth between $(Bi_2O_2)^{2+}$ sheets and $(A_{m-1}B_mO_{3m+1})^{2-}$ perovskite-like layers containing from $m=$ 1–8 layers.[2–4] Anionic conductivity is the result of oxygen vacancies, either intrinsic as in $Bi_2VO_{5.5}$ and related BIMEVOX compounds,[5–18] or extrinsic when these vacancies are introduced by appropriate dopants with lower valence states.[19–23]

We recently succeeded in preparing Bi_2WO_6 ($m=1$) oxygen deficient phases by substitution for W^{VI} with Nb^V and Ta^V, thus leading to $Bi_2W_{1-x}M_xO_{6-x/2}$ solid solutions within the composition range $0 < x < 0.15$. Maximum oxide ion conductivities were obtained when $x=0.05$ for both phases and reached conductivity values of $10^{-3}\ \Omega^{-1}\,cm^{-1}$ at *ca.* 450 °C. These performances are intermediate between those of the high anion conductor BIMEVOX phases and those of doped higher members of the Aurivillius series $m=2$, 3 and 4.[24]

Bi_2WO_6 is a displacive ferroelectric compound having a rather complicated structure at 298 K, which has engendered some controversy but, from the most recent refinement,[25,26] its actual structure can be described as a combination of commensurate modulations of an idealised *Fmmm* parent structure derived from the prototype *I*4/*mmm* structure. The different displacive modes reduce the space group symmetry of each mode and are associated with important atomic displacements from the prototype: rotations of the WO_6 octahedra together with lateral displacements of these octahedra and of the other atoms. All these modulations create some degree of covalency between Bi and some O apical atoms of the WO_6 octahedra and ensure stabilisation of the structure.[27] A simpler but valuable description using only one space group $Pca2_1$ was also provided recently from powder neutron diffraction.[28] In both descriptions, chemical bond lengths and bond angles are practically identical and for obvious reasons of simplicity, the second description will be used as a starting point in our study.

* E-mail: mairesse@ensc-lille.fr

The present paper deals with a neutron powder diffraction investigation of the doped phases along with computer simulation methods to clarify some of the factors controlling oxygen transport in these materials. These simulation techniques are particularly suited to probing ion migration on the atomic scale and have been successfully applied to other anionic conductors such as perovskite-based oxides[29] and brownmillerite-structured $Ba_2In_2O_5$.[30] In this work the energetics of extrinsic defects and of various mechanisms or pathways for oxygen migration have been explored and compared with the experimental structural and conductivity data.

Methods

Experimental

Polycrystalline samples were prepared by solid state reactions from appropriate amounts of stoichiometric mixtures as previously described.[24] They were characterised by X-ray diffraction with a Guinier De Wolff focusing camera using Cu-Kα radiation, to check their purity before neutron diffraction measurements.

Neutron diffraction data were collected at room temperature on the high resolution powder diffractometer D1A at the Institut Laue Langevin (ILL) at Grenoble. Approximately 40 g of each sample were placed in a 15 mm diameter cylindrical vanadium can and data were collected in the range $0 < 2\theta \leqslant 158.45^{\circ}$ at a wavelength of $\lambda = 1.909$ Å; only data in the range $10 \leqslant 2\theta \leqslant 150^{\circ}$ were used in the refinement. The detector bank was stepped in intervals of 0.05° in 2θ and the resulting data were normalised with respect to detector efficiency and positional errors. The data were refined using the Fullprof program.[31] As tungsten has a significant absorption cross-section of $18.4 \times 10^{-24}\ cm^2$, absorption correction has been performed.

Atomistic simulation

The simulation techniques are based upon energy minimisation procedures and the Mott–Littleton methodology for accurate modelling of perfect and defective lattices. Detailed reviews of

these well established techniques are given elsewhere,[32,33] so only a brief account will be presented here.

An important feature of these calculations is the treatment of lattice relaxation about the point defect or dopant ion. The Mott–Littleton approach is to divide the crystal lattice into two regions so that ions in a spherical inner region surrounding the defect are relaxed explicitly. In contrast, the remainder of the crystal, where the defect forces are relatively weak, is treated by the Mott–Littleton approximation.[32,33] In this way local relaxation is modelled effectively, so the crystal is not considered simply as a rigid lattice through which oxygen ions can migrate.

There is now ample evidence that given reliable interatomic potentials and a sufficiently large inner region these methods can yield accurate values of the energies of defect formation, migration and substitution.[33] The interatomic interactions are divided into long-range Coulombic and short-range forces, with the short-range term represented by pairwise potentials of the form:

$$\varphi_{ij}(r) = A_{ij}\exp(-r/\rho_{ij}) - C_{ij}/r^6$$

where A_{ij}, ρ_{ij} and C_{ij} are potential parameters assigned to each ion–ion interaction. The simulation model also incorporates the shell model to describe both ionic polarisation and the effect that polarisation has in modifying the effective overlap interactions. Shell model potentials have proven to be effective in simulating the dielectric properties of ceramic oxides. In general, these simulation methods have been applied to a rich variety of solid state materials including recent studies of defects and oxygen ion transport in ternary oxides.[29,30]

Results and Discussion

Neutron diffraction

In order to use Bi_2WO_6 as a reference, Rietveld refinement of the neutron powder diffraction data on this phase was performed in the space group $Pca2_1$ from the starting model previously mentioned.[28] A first refinement was carried out with an independent isotropic thermal parameter for each atom and led to the results reported in Table 1(*a*). These results are in very good agreement with those of ref. 28. Then, to take into account the similar structural roles of some atoms in the crystal structure, a second refinement was performed where the thermal parameters of some atom pairs were constrained to be equal: Bi(1) and Bi(2), O(2) and O(3) oxygen atoms of the Bi_2O_2 sheets, O(1) and O(6) apical oxygen atoms within one WO_6 octahedron, O(4) and O(5) equatorial oxygen atoms within the same octahedron. The corresponding results are reported in Table 1(*b*) and the atom labelling within one WO_6 octahedron is depicted on Fig. 1. Both refinements yield similar atomic coordinates within the experimental uncertainty but the second one provides a more homogeneous description in term of crystal chemistry. The corresponding *B* values were used in the refinement of the doped phases as fixed parameters but the occupancy factors of all atom pairs, except Bi(1) and Bi(2) were allowed to vary.

Table 1 Bi_2WO_6 parameters refined (*a*) without constraint on thermal parameters and (*b*) refined with B [O(1)] = B [O(6)], B [O(2)] = B [O(3)] and B [O(4)] = B [O(5)]

atom	*x*	*y*	*z*	*B*/Å^2
Bi(1)	0.5204(6)	0.4226(2)	0.983(2)	0.69(7)
Bi(2)	0.4813(6)	0.0781(2)	0.977(1)	0.96(7)
W	0.001(2)	0.2513(6)	0	0.74(6)
O(1)	0.057(2)	0.1398(6)	0.073(2)	0.6(2)
O(2)	0.2586(7)	0.0007(4)	0.268(2)	0.7(2)
O(3)	0.2380(7)	0.4991(4)	0.260(2)	0.9(2)
O(4)	0.7056(9)	0.2330(4)	0.256(2)	1.12(9)
O(5)	0.2124(9)	0.2647(4)	0.334(2)	1.23(9)
O(6)	0.561(2)	0.3601(7)	0.573(2)	2.0(2)

a = 5.4365(1) Å, b = 16.4333(3) Å, c = 5.4577(2) Å; R_p = 4.14%, R_{wp} = 5.34%, R_E = 2.44%, R_F = 2.21%, R_B = 3.19%.

atom	*x*	*y*	*z*	*B*/Å^2
Bi(1)	0.5204(6)	0.4226(2)	0.980(2)	0.82(2)
Bi(2)	0.4812(5)	0.0781(2)	0.979(2)	0.82(2)
W	0.001(2)	0.2521(5)	0	0.72(5)
O(1)	0.054(2)	0.1397(6)	0.078(2)	1.22(4)
O(2)	0.2586(6)	0.0006(4)	0.267(1)	0.80(3)
O(3)	0.2381(6)	0.4993(4)	0.260(1)	0.80(3)
O(4)	0.7053(9)	0.2331(4)	0.255(2)	1.15(4)
O(5)	0.2132(9)	0.2646(4)	0.334(2)	1.15(4)
O(6)	0.563(2)	0.3600(6)	0.567(1)	1.22(4)

a = 5.4365(1) Å, b = 16.4333(3) Å, c = 5.4577(1) Å; R_p = 4.15%, R_{wp} = 5.34%, R_E = 2.44%, R_F = 2.14%, R_B = 3.15%.

Typical results of such a refinement strategy, based on the assumption that doping of Bi_2WO_6 would not significantly modify the parent crystal structure, are reported in Table 2 and Fig. 2. The most striking features are as follows: (*a*) when compared with undoped Bi_2WO_6 [Table 1(*b*)] the atomic coordinates are indeed very similar in both compounds. (*b*) The W/Ta ratio is in very good agreement with the formal composition. (*c*) The occupancy of the O(2) and O(3) oxygen sites of the Bi_2O_2 sheets is very close to unity while the occupancies of the WO_6 oxygen sites are slightly lower but similar, indicating that the oxygen vacancies are likely only located within the perovskite-like slab and randomly distributed among the apical and equatorial positions in the WO_6 octahedral oxygen surrounding. Nevertheless, owing to the small amount of vacancy, the reliability factors do not significantly change when O sites are assumed to be fully occupied. (*d*) The oxygen stoichiometry resulting from oxygen occupancy site summation is 5.92 or 5.94 when considering a value of unity for O(2) and O(3).This value is again in very good agreement with the expected value of 5.95.

All these consistent experimental data enable us to have confidence in the results from neutron powder diffraction data despite the small degree of doping. Similar results corresponding to a 5% doping level with Ta and Nb are presented in Table 3. The W/M ratio and oxygen stoichiometry are in agreement with the expected formula but this time the low amount of dopant precludes characterisation of oxygen vacancies.

The main bond lengths in the doped and undoped phases are reported in Table 4 and the shortest O—O distances within one WO_6 octahedron always involve an apical oxygen position O(1) or O(6) associated with an equatorial atom O(4) or O(5), which should indicate a preferred oxygen jump between these two different sites.

Structural modelling

A crucial test of any theoretical study of solid state materials is the accurate simulation of the crystal structure. The starting

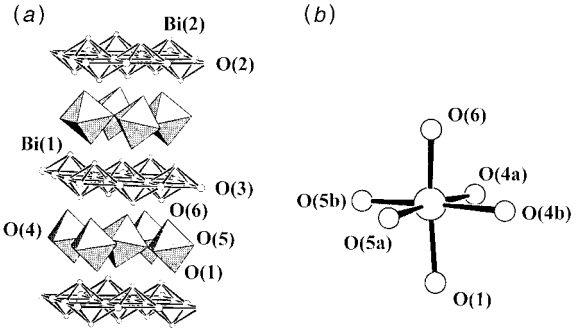

Fig. 1 Labelling of the atoms (*a*) in one cell, (*b*) in an octahedron

Table 2 $Bi_2W_{0.90}Ta_{0.10}O_{5.95}$ parameters

atom	x	y	z	B/Å^2	occupancy
Bi(1)	0.5201(7)	0.4231(3)	0.980(2)	1.05(3)	1
Bi(2)	0.4819(7)	0.0788(3)	0.972(2)	1.05(3)	1
W/Ta	0.001(2)	0.2530(6)	0	0.72	0.91/0.09(2)
O(1)	0.057(2)	0.1402(5)	0.074(2)	1.22	0.985(4)
O(2)	0.2573(7)	0.0003(5)	0.265(2)	0.80	0.992(4)
O(3)	0.2390(7)	0.4997(5)	0.256(2)	0.80	0.992(4)
O(4)	0.706(1)	0.2317(4)	0.250(2)	1.15	0.984(4)
O(5)	0.2182(9)	0.2639(4)	0.323(2)	1.15	0.984(4)
O(6)	0.562(2)	0.3617(5)	0.561(2)	1.22	0.985(4)

$a=5.4385(1)$ Å, $b=16.4552(3)$ Å, $c=5.4614(1)$Å; $R_p=4.44\%$, $R_{wp}=5.61\%$, $R_E=1.90\%$, $R_F=3.27\%$, $R_B=4.34\%$.

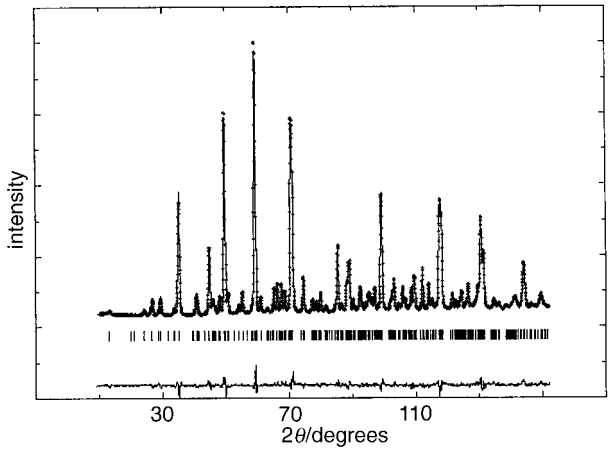

Fig. 2 Observed and calculated neutron powder diffraction patterns of $Bi_2W_{0.90}Ta_{0.10}O_{5.95}$. The difference pattern appears in the lower part.

Table 3 $Bi_2W_{1-x}M_xO_{6-0.5x}$ occupancies

	M = Nb, $x=0.05$	M = Ta, $x=0.05$	M = Ta, $x=0.10$
W/M	0.96/0.04(2)	0.94/0.06(2)	0.91/0.09(2)
O(1)/O(6)	0.991(3)	1.014(4)	0.985(4)
O(4)/O(5)	1.002(3)	1.022(4)	0.984(4)
O total	5.98	6	5.94
O expected	5.975	5.975	5.95
R_p (%)	4.07	4.47	4.44
R_{wp} (%)	5.30	5.73	5.61
R_E (%)	2.05	2.87	1.90
R_B (%)	3.21	3.62	4.34
R_F (%)	2.16	2.73	3.27

point for our investigation of Bi_2WO_6 was the crystal structure model of Knight;[28] as already noted, our neutron diffraction results agree well with this study. The short-range interatomic potentials were transferred directly from recent simulations of $Bi_2Mo_2O_9$.[34] All the cations are assigned formal charges which has the advantage of allowing a clear distinction between isovalent and aliovalent dopant substitution. Details of the potentials and shell model parameters used in this study are given in Table 5.

By using efficient energy minimisation procedures, the unit cell dimensions and ion positions were allowed to equilibrate under constant pressure conditions. The resulting lattice parameters are compared with our experimental values in Table 6. This clearly reveals good agreement between simulated and observed structures of Bi_2WO_6 without the need for further empirical refinement for this system. The interatomic potential model for Bi_2WO_6, therefore, provides a good basis for the defect calculations.

Dopant substitution calculations

It has been established that the incorporation of aliovalent cations (especially Ta^V and Nb^V) is crucial to the ionic conductivity of Bi_2WO_6. However, from diffraction studies direct sensitivity to substitution into oxide structures that have two metal sites can be difficult. Our simulation approach is based on assessing the relative energetics of reaction (or solution) for dopant substitution into the host lattice. For Bi_2WO_6, the most important mode of incorporation is as a substitutional at the W^{VI} site with the creation of extrinsic oxygen vacancies. This may be described by defect reactions; for example, the substitution of M^V cations for W^{VI} can be written as:

$$M_2O_5 + 2W^X_W + O^X_O \rightarrow 2M'_W + V^{\cdot\cdot}_O + 2WO_3$$

where M'_W signifies a dopant substitutional and $V^{\cdot\cdot}_O$ an oxygen vacancy. The energies of solution are then evaluated by combining appropriate defect and lattice energy terms. We note that the interatomic potentials for the dopant species are exactly those of previous modelling studies of corresponding oxides,[29,35–38] most of which have been applied to similar dopant calculations in other host materials. The resulting energies for a range of dopant ions on both W and Bi sites are presented in Table 7.

Three main points emerge from these results. First, the most favourable solution energies at the W site and hence the highest solubilities are clearly found for Nb^V and Ta^V. This agrees well with observation as it is known that Nb_2O_5 and Ta_2O_5 readily dissolve into the W sublattice of Bi_2WO_6 to form solid solutions with higher ionic conductivity.[24] A low solution energy is also predicted for Zr^{IV} on W which is worth further experimental investigation.

Second, substitution at the Bi site is generally unfavourable except for the La^{III} and Mn^{III} ions, which is consistent with the available experimental data. Watanabe and Inoue[39–41] described two solid solutions in the binary diagram Bi_2WO_6–La_2WO_6, one of which is based on the Bi_2WO_6 structure and forms up to $x=0.2$ in $Bi_{2-x}La_xWO_6$. However, since these dopants do not yield charge-compensating defects, it is unlikely that they will enhance the ion transport.

Finally, in the case of the other dopant ions (including Cu^{II}), we calculate relatively unfavourable solution energies. This may explain the limited solubility of these ions in Bi_2WO_6 and the formation of mixed-phase systems, as experimentally demonstrated for Cu addition.[42] In contrast, the related $Bi_4V_2O_{11}$ material can accommodate a rich variety of lower-valence cations to form the widely studied BIMEVOX family of compounds.[5–18] We should note that although Jahn–Teller effects of the Cu^{II} (d^9) dopant are not included explicitly in our atomistic approach, the corresponding potentials have been particularly successful in modelling studies of the high T_c cuprate superconductors,[36,38] which provides support for their general validity.

Table 4 Undoped and doped Bi_2WO_6 main bond lengths with shortest O—O distances in italics

	Bi_2WO_6	$Bi_2W_{0.95}Ta_{0.05}O_{5.975}$	$Bi_2W_{0.90}Ta_{0.10}O_{5.95}$	$Bi_2W_{0.95}Nb_{0.05}O_{5.975}$
Bi(1)—O(3)[a]	2.49(1)	2.51(1)	2.49(1)	2.51(1)
Bi(1)—O(3)[b]	2.24(1)	2.23(1)	2.25(1)	2.24(1)
Bi(1)—O(3)[c]	2.31(1)	2.34(1)	2.30(1)	2.32(1)
Bi(1)—O(3)[d]	2.21(1)	2.18(1)	2.19(1)	2.18(1)
Bi(1)—O(6)[a]	2.47(1)	2.46(1)	2.51(1)	2.47(1)
Bi(1)—O(6)[b]	2.54(1)	2.57(1)	2.53(1)	2.55(1)
Bi(2)—O(2)[a]	2.36(1)	2.34(1)	2.39(1)	2.35(1)
Bi(2)—O(2)[b]	2.15(1)	2.15(1)	2.16(1)	2.17(1)
Bi(2)—O(2)[c]	2.54(1)	2.55(1)	2.54(1)	2.53(1)
Bi(2)—O(2)[d]	2.23(1)	2.25(1)	2.23(1)	2.23(1)
Bi(2)—O(1)[a]	2.58(1)	2.54(1)	2.58(1)	2.56(1)
Bi(2)—O(1)[b]	2.44(1)	2.45(1)	2.41(1)	2.44(1)
W(M)—O(1)[a]	1.91(2)	1.92(1)	1.92(2)	1.92(2)
W(M)—O(4)[a]	2.15(1)	2.16(1)	2.13(1)	2.17(1)
W(M)—O(4)[b]	1.78(1)	1.79(1)	1.80(1)	1.79(1)
W(M)—O(5)[a]	2.16(1)	2.15(1)	2.13(1)	2.14(1)
W(M)—O(5)[b]	1.81(1)	1.80(1)	1.82(1)	1.79(1)
W(M)—O(6)[b]	1.86(2)	1.85(1)	1.85(2)	1.84(2)
O(1)—O(4)[a]	*2.64(1)*	*2.64(1)*	*2.62(1)*	*2.64(1)*
O(1)—O(4)[b]	2.72(1)	2.73(1)	2.73(1)	2.72(1)
O(1)—O(5)[a]	*2.63(1)*	*2.57(1)*	*2.60(1)*	*2.61(1)*
O(1)—O(5)[b]	2.73(1)	2.68(1)	2.74(1)	2.74(1)
O(4)—O(4)[b]	2.77(1)	2.78(1)	2.77(1)	2.78(1)
O(4)—O(5)[a]	2.84(1)	2.87(1)	2.86(1)	2.86(1)
O(4)—O(5)[a]	2.76(1)	2.73(1)	2.73(1)	2.74(1)
O(5)—O(5)[b]	2.76(1)	2.75(1)	2.75(1)	2.76(1)
O(6)—O(4)[a]	2.83(2)	2.87(1)	2.84(1)	2.82(1)
O(6)—O(4)[b]	*2.64(2)*	*2.73(1)*	*2.69(1)*	*2.67(1)*
O(6)—O(5)[a]	2.79(2)	2.77(1)	2.79(1)	2.77(1)
O(6)—O(5)[b]	*2.59(2)*	*2.63(1)*	*2.64(1)*	*2.61(1)*
O(2)—O(2)[b]	2.73(1)	2.73(1)	2.73(1)	2.73(1)
O(2)—O(2)[c]	2.72(1)	2.72(1)	2.72(1)	2.72(1)
O(3)—O(3)[b]	2.73(1)	2.73(1)	2.73(1)	2.73(1)
O(3)—O(3)[c]	2.72(1)	2.72(1)	2.72(1)	2.72(1)

Symmetry operators: [a] x, y, z. [b] $1/2-x, y, 1/2+z$. [c] $x+1/2, -y, z$. [d] $-x, -y, 1/2+z$.

Table 5 Interatomic potentials for Bi_2WO_6

(*a*) short-range

interaction	A/eV	ρ/Å	C/eV Å^6
$Bi^{3+}\cdots Bi^{3+}$	24244.5	0.3284	0.0
$Bi^{3+}\cdots O^{2-}$	49529.35	0.2223	0.0
$W^{6+}\cdots O^{2-}$	767.43	0.4386	0.0
$O^{2-}\cdots O^{2-}$	9547.96	0.2192	32.0

(*b*) shell model

species	Y/e	k/eV Å^{-2}
Bi^{3+}	−5.51	359.55
W^{6+}	5.89	7.69
O^{2-}	−2.04	6.3

Table 6 Calculated and experimental lattice parameters for Bi_2WO_6

parameter	calc.	exptl. (this study)
a/Å	5.4113	5.4365
b/Å	16.7710	16.4333
c/Å	5.5340	5.4577

Perhaps the most significant conclusion from these substitution calculations is that Nb^V and Ta^V solubility in Bi_2WO_6 is expected to be favourable owing to their low heats of solution. Solution of Nb^V and Ta^V will therefore enhance the oxygen diffusivity owing to the increase in the concentration of oxygen vacancies.

It is well known that for many anion conducting oxides the conductivity is affected by the extent of dopant–vacancy association. This can be described in terms of the formation of simple pair clusters for low dopant concentrations and reduced temperatures, which add a binding energy term to the Arrhenius energy of the ionic conductivity. Consequently, we have considered pair clusters in the Bi_2WO_6 system comprised of a dopant ion and an oxygen vacancy at nearest-neighbour positions. We decided to focus our attention on the formation of Ta-vacancy clusters, although several calculations for the Nb dopant produced very similar trends.

Calculations were performed on pair clusters comprised of Ta'_w substitutionals and neighbouring O(1, 4, 5 or 6) vacancies. The binding energies (with respect to the isolated defects) reveal that the pair clusters are bound when the oxygen vacancy is located at all the nearest-neighbour octahedron sites, with a mean binding energy of 0.25 eV. We recognise that further investigations need to consider other configurations which may have greater stability particularly at higher dopant concentrations. Nevertheless, these results suggest a

Table 7 Calculated energies of solution (eV) for cation dopants at both W and Bi sites

Dopant ion	W site	Bi site
Co^{II}	1.82[a]	2.52
Cu^{II}	1.39[a]	2.07
Mn^{III}	5.88	0.81
Fe^{III}	3.62	1.35
La^{III}	6.04	−2.21
Bi^{III}	5.24[a]	—
Zr^{IV}	0.05	nc
Ti^{IV}	2.23	nc
V^V	14.49	26.3
Ta^V	−1.65	7.65
Nb^V	−1.13	7.60
W^{VI}	—	16.22

[a]Non-convergence (nc) for calculation of isolated dopant; energy derived from cluster with oxygen vacancies.

tendency toward defect association and a less random distribution in Ta-doped Bi_2WO_6 which would inhibit oxygen ion mobility. It is worth noting that the magnitude of the binding energy is comparable to values found for pair clusters in other oxygen ion conductors such as lanthanide doped CeO_2.[33]

Our recent impedance measurements on Ta-doped Bi_2WO_6[24] show a small, reversible slope change in the conductivity curves at *ca.* 550 °C. It was proposed that the slope change may be correlated with an order–disorder phase transition owing to the existence of dopant–vacancy pair interactions at low temperature; this observation is compatible with the cluster calculations in the present study, a point to which we return below.

Oxygen vacancy migration

Ionic conductivity in doped Bi_2WO_6 depends on the migration of extrinsic oxygen vacancies through the lattice. However, despite the evident implications for transport behaviour, the precise nature of the migration mechanism or pathway is still uncertain. Simulation methods can greatly enhance our understanding of this problem by evaluating the activation energies for various defect mechanisms at the atomic level.

For the Bi_2WO_6 structure (Fig. 1) there are a number of possible migration mechanisms or jumps between neighbouring oxygen positions within the WO_6 octahedra and the Bi_2O_2 sheets. The migration energies were evaluated from energy profiles by calculating the dopant energy of the migrating anion along the diffusion path between adjacent oxygen sites. In this way the 'saddle-point' configuration can be identified from which the energy barrier to migration is derived. The resulting migration energies for a range of oxygen vacancy jumps are reported in Table 8.

Examination of the results reveals high energy barriers (>1.6 eV) to oxygen ion migration within the Bi_2O_2 sheets and along the [WO_6] equatorial plane; this suggests that such pathways would have a negligible contribution to oxygen transport. We find a possible low energy pathway involves a zigzag type mechanism between adjacent apical O(1,6) and equatorial O(4, 5) sites, with an alternating sequence of migration energies of 0.45 and 0.63 eV. In view of this type of motion, highly anisotropic ionic conductivity is expected with a migration energy of 0.63 eV. This calculated value is consistent with the observed values of 0.50 and 0.54 eV for $Bi_2W_{1-x}Nb_xO_{6-x/2}$ and $Bi_2W_{1-x}Ta_xO_{6-x/2}$ respectively at high temperatures ($x=0.05$, $T > 550$ °C),[24] where defect association is believed to be less significant.

The calculated migration energy of 0.63 eV relates purely to oxygen vacancy jumps and does not include explicitly the effects of defect association. However, as already noted, the formation of dopant–vacancy (Ta_W V_O) clusters adds a term equal to the binding energy to the Arrhenius energy of the conductivity. With our calculated binding energy of 0.25 eV, this leads to an activation energy of 0.88 eV which correlates well with experimental values of 0.78–0.86 eV for Bi_2W_{1-x}(Nb or Ta)$_xO_{6-x/2}$ from measurements at temperatures below 450 °C.[24] Moreover, this result lends further support to the view that the observed slope change in the conductivity is related to dopant–vacancy association at low temperature.

Table 8 Energies for oxygen vacancy migration

migration pathway[a]	E_{mig}/eV
WO_6 (apical–equatorial)	
O(1)—O(4a)	0.97
O(1)—O(4b)	0.45
Q(1)—O(5a)	1.73
O(1)—O(5b)	0.63
O(6)—O(4a)	0.63
O(6)—O(4b)	1.73
O(6)—O(5a)	0.45
O(6)—O(5b)	0.97
WO_6 (equatorial–equatorial)	
O(4a)—O(4b)	1.67
O(4a)—O(5b)	1.61
O(4b)—O(5a)	2.71
O(5a)—O(5b)	1.67
Bi_2O_2 sheets	
O(2)—O(2)	1.60
O(3)—O(3)	1.60

[a]See Fig. 1 for oxygen sites.

Conclusion

A combination of neutron diffraction and computer simulation techniques has yielded valuable information on the structural and transport properties of the Bi_2WO_6 based oxygen ion conductor. The following conclusions have emerged from our study.

(1) The perfect lattice simulations, based on our interatomic potential model, revealed good agreement between the observed and calculated structures of Bi_2WO_6.

(2) Neutron diffraction data show that oxygen vacancies introduced by doping are randomly distributed among the apical and equatorial positions within the perovskite-like slab.

(3) The most energetically favourable dopant substitution is predicted for Nb^V and Ta^V on W^{VI} and La^{III} on Bi^{III}, which agrees well with the solid solutions that have been synthesised successfully. Incorporation of Nb^V and Ta^V will enhance the oxygen diffusivity owing to the increase in the oxygen vacancy concentration. However, the relatively unfavourable energetics for most dopants indicate much less solubility for lower-valence cations into Bi_2WO_6, in contrast to the extensively doped $Bi_4V_2O_{11}$ (BIMEVOX) system.

(4) The lowest energy pathway for oxygen vacancy migration involves a zigzag type mechanism between adjacent apical O(1,6) and equatorial O(4,5) sites of the WO_6 octahedra; the mean migration energy of 0.63 eV is in agreement with our observed values for Ta- and Nb-doped Bi_2WO_6 at high temperatures (>550 °C).

(5) Pair clusters comprised of a Ta'_W substitutional and a neighbouring O(1,4,5 or 6) vacancy are predicted to form with a mean binding energy of 0.25 eV. This calculated binding term leads to an effective activation energy for oxygen vacancy migration of 0.88 eV, which correlates well with our experimental values for Bi_2W_{1-x}(Nb or Ta)$_xO_{6-x/2}$ at temperatures below 450 °C. It is proposed that the observed slope change in the ionic conductivity plots is related to dopant–vacancy association at low temperature.

Future work will encompass molecular dynamics (MD) simulations of oxygen diffusion in doped Bi_2WO_6 and will be extended to joint experimental–computational studies of the γ-$Bi_4V_2O_{11}$ material.

The Institut Laue Langevin is thanked for providing neutron facilities and Dr. Emmanuelle Suard (Institut Laue Langevin) is gratefully acknowledged for helpful discussions.

References

1 K. R. Kendall, C. Navas, J. K. Thomas and H. C. zur Loye, *Chem. Mater.*, 1996, **8**, 642 and references therein.
2 B. Aurivillius, *Ark. Kemi.*, 1949, **1**, 463; 499; 1949, **2**, 519.
3 J. L. Hutchison, J. S. Anderson and C. N. R. Rao, *Proc. R. Soc. London, Ser. A*, 1977, **355**, 301.
4 B. Frit and J. P. Mercurio, *J. Alloys Compd.*, 1992, **188**, 27.
5 F. Abraham, M. F. Debreuille-Gresse, G. Mairesse and G. Nowogrocki, *Solid State Ionics*, 1988, **28/30**, 529.
6 F. Abraham, J. C. Boivin, G. Mairesse and G. Nowogrocki, *Solid State Ionics*, 1990, **40/41**, 934.

7 K. B. R. Varma, G. N. Subbanna, T. N. Guru Rao and C. N. R. Rao, *J. Mater. Res*., 1990, **5**, 2718.
8 J. B. Goodenough, A. Manthiram, M. Paranthaman and Y. S. Zhen, *Mater. Sci. Eng. B*, 1992, **12**, 357; *Solid State Ionics*, 1992, **52**, 105.
9 G. Mairesse, in *Fast Ion Transport in Solids*, ed. B. Scrosati, Kluwer, Dordrecht, 1993, p. 271.
10 O. Joubert, A. Jouanneaux, M. Ganne, R. N. Vannier and G. Mairesse, *Solid State Ionics*, 1994, **73**, 309.
11 C. K. Lee, M. P. Tam and A. R. West, *J. Mater. Chem*., 1994, **4**, 525.
12 C. K. Lee, G. S. Lim and A. R. West, *J. Mater. Chem*., 1994, **4**, 1441.
13 J. Yan and M. Greenblatt, *Solid State Ionics*, 1995, **81**, 225.
14 J. R. Dygas, F. Krok, W. Bogusz, P. Kurek, K. Reiselhuber and M. W. Breiter, *Solid State Ionics*, 1994, **70/71**, 239.
15 S. Lazure, R. N. Vannier, G. Nowogrocki, C. Muller, M. Anne and P. Strobel, *J. Mater. Chem*., 1995, **5**, 1395.
16 P. Shuk, H.-D. Wiemhöfer, U. Guth, W. Göpel and M. Greenblatt, *Solid State Ionics*, 1996, **89**, 179 and references therein.
17 S. Lazure, C. Vernochet, R. N. Vannier, G. Nowogrocki and G. Mairesse, *Solid State Ionics*, 1996, **90**, 117.
18 Y. L. Yang, L. Qiu, W. T. A. Harrison, R. Christoffersen and A. J. Jacobson, *J. Mater. Chem*., 1997, **7**, 243.
19 A. Q. Pham, M. Puri, J. F. Dicarlo and A. J. Jacobson, *Solid State Ionics*, 1994, **72**, 309.
20 A. Q. Pham, I. Yazdi and A. J. Jacobson, *J. Electrochem. Soc*., 1995, **142**, 1559.
21 K. R. Kendall, J. K. Thomas and H. C. zur Loye, *Solid State Ionics*, 1994, **70/71**, 221.
22 K. R. Kendall, J. K. Thomas and H. C. zur Loye, *Chem. Mater*., 1995, **7**, 50.
23 J. K. Thomas, K. R. Kendall and H. C. zur Loye, *Solid State Ionics*. 1994, **70/71**, 225.
24 N. Baux, R.N. Vannier, G. Mairesse and G. Nowogrocki, *Solid State Ionics*, 1996, **91**, 243.
25 J. G. Thompson, S. Schmid, R. L. Withers, A. D. Rae and J. D. Fitzgerald, *J. Solid State Chem*., 1992, **101**, 309.
26 A. D. Rae, J. G. Thompson and R. L. Withers, *Acta Crystallogr., Sect. B*, 1991, **47**, 870.
27 S. Seong, K. A. Yee and T. A. Albright, *J. Am. Chem. Soc*., 1981, **115**, 1981.
28 K. S. Knight, *Mineral. Mag*., 1992, **56**, 399.
29 M. Cherry, M. S. Islam and C. R. A. Catlow, *J. Solid State Chem*., 1995, **118**, 125.
30 C. A. J. Fisher, M. S. Islam and R. J. Brook, *J. Solid State Chem*., 1997, **128**, 137.
31 J. Rodriguez-Carjaval, Program Fullprof, version 2.4, 1993.
32 *Computer Simulation of Solids*, ed. C. R. A. Catlow and W. C. Mackrodt, Lecture Notes in Physics 166, Springer-Verlag, Berlin, 1982.
33 C. R. A. Catlow, in *Solid State Chemistry: Techniques*, ed. A. K. Cheetham and P. Day, Clarendon Press, Oxford, 1987.
34 M. Cherry, PhD Thesis, University of Surrey, 1996.
35 G. V. Lewis and C. R. A. Catlow, *J. Phys. C*, 1985, **18**, 1149.
36 M. S. Islam and L. J. Winch, *Phys. Rev. B*, 1995, **52**, 10 510; D. J. Ilett and M. S. Islam, *J.Chem. Soc., Faraday Trans*., 1993, **89**, 3833.
37 M. Exner, H. Donnerberg, C. R. A. Catlow and O. F. Schirmer, *Phys. Rev. B*, 1995, **52**, 3930.
38 R. C. Baetzold, *Phys. Rev. B*, 1995, **48**, 5789.
39 A. Watanabe, *Mater. Res. Bull*., 1980, **15,** 1473.
40 A. Watanabe, Z. Inoue and T. Ohsaka, *Mater. Res. Bull*., 1980. **15**, 397.
41 A. Watanabe and Z. Inoue, *J. Mater. Sci*., 1980, **15,** 2669.
42 R. N. Vannier, G. Nowogrocki and G. Mairesse, *J. Mater. Chem*., 1995, **5**, 361.

Paper 7/07221J; *Received* 6*th October*, 1997